Eur. Phys. J. A (2025) 61:51
https://doi.org/10.1140/epja/s10050-025-01509-5

THE EUROPEAN PHYSICAL JOURNAL A

Regular Article - Experimental Physics

Plasma-delay studies on heavy ion detection using PIPS at the LOHENGRIN recoil separator

Ana M. Gómez L. [1,a], **Ali Al-Adili**[1,b], **Diego Tarrío**[1], **Andreas Solders**[1], **Zhihao Gao**[1], **Alf Göök**[1], **Stephan Pomp**[1], **André Poussette**[1], **Samuel Bennett**[5], **Yung Hee Kim**[3], **Ulli Köster**[3], **Andreas Oberstedt**[6], **Gavin Smith**[5], **Nikolay V. Sosnin**[4,5], **Stephan Oberstedt**[2]

[1] Department of Physics and Astronomy, Uppsala University, Box 516, 751 20 Uppsala, Sweden
[2] European Commission, Joint Research Centre (JRC), 2440 Geel, Belgium
[3] Present affiliation: Center for Exotic Nuclear Studies, Institute of Basic Science, Daejeon (34126), Republic of Korea
[4] University of Edinburgh, Edinburgh EH9 3FD, UK
[5] University of Manchester, Manchester M13 9PL, UK
[6] Extreme Light Infrastructure - Nuclear Physics (ELI-NP), Horia Hulubei National Institute for R&D in Physics and Nuclear Engineering (IFIN-HH), 077125 Bucharest-Magurele, Romania

Received: 28 July 2024 / Accepted: 9 February 2025

Communicated by Alexandre Obertelli

Abstract The VERDI fission spectrometer is designed to measure fragment velocities and kinetic energies to achieve high-precision yield measurements. It consists of two time-of-flight (TOF) sections, each hosting a micro-channel plate (MCP) and up to 32 passivated implanted planar silicon (PIPS) detectors. The main challenge to achieve accurate fragment velocities is the so-called plasma delay time (PDT) phenomena in the PIPS detectors. In this work, we present a dedicated experimental campaign at the LOHENGRIN fission-fragment recoil separator, to solve the pending PDT challenges. The PDT effect was systematically investigated, as a function of mass and energy, using a dedicated time-of-flight setup. In addition, the pulse height defect (PHD) was determined simultaneously. The studies were conducted for five PIPS detectors, in energies and mass numbers ranging from 20 to 110 MeV and A = 85 to 149, respectively. Using digital signal processing, an excellent timing resolution was achieved, reaching as low as 60 ps (one σ) for the heavy ions. The PDT revealed a strong positive correlation with the ion energy and a weak negative correlation with the mass. The experimental PDT values determined from five detectors confirm a consistent systematic behavior with respect to mass and energy. Some systematic discrepancies were exhibited by two detectors, possibly due to the use of different pre-amplification chains. The PDT measurements ranged between 1 and 3.5 ns, for heavy ions relative to α-particles. The PHD values showed also a strong correlation with the ion energy, and moreover with the ion mass. The PHD for heavy ions was found to range between 2 and 8 MeV, relative to α-particles. Finally, a two-dimensional parameterisation was developed to model the experimental PDT data, as a function of mass and energy. This new model, which is valid in the fission fragment mass and energy regime, will be of benefit for heavy-ion velocity measurements, using silicon detectors, as done in VERDI.

1 Introduction

VERDI (VElocity foR Direct particle Identification) is a spectrometer designed for precise measurements of the fission-fragment (FF) mass and energy distributions [1,2]. The measurement technique is based on the so-called double-energy double-velocity (2E-2v) method, which allows the determination of both pre- and post-neutron emission mass yields. With a contemplated mass-resolving power between 1 and 2 atomic mass units, the technique promises high-precision fission data, vital for both nuclear applications and fission-model development. Moreover, the spectrometer facilitates the determination of the fragment-specific average neutron emission multiplicity, $\bar{\nu}(A)$. This serves as a valuable complement to other detection techniques, enabling independent examination of excitation-energy sharing in nuclear fission [3]. VERDI consists of two arms, each hosting one micro-channel plate detector (MCP) and up to 32 passivated implanted planar silicon (PIPS) detectors. Fragment velocities are calculated from times-of-flight measured using

[a] e-mail: ana.gomez@physics.uu.se (corresponding author)
[b] e-mail: ali.al-adili@physics.uu.se (corresponding author)

Published online: 15 March 2025

timing signals from MCPs (start signals) and PIPS detectors (stop signals), with the latter also providing kinetic energy measurements of fission products. While MCPs are fast and could potentially provide both start and stop timing signals, using an additional MCP for stop timing would require an intermediate foil, leading to energy loss and scattering that degrade energy and mass resolution. Another factor is the geometrical efficiency, which would be compromised if a foil were placed at the end of the flight path, as the foil's area cannot be made excessively large. Alternatives such as single-crystal diamond (sCVD) detectors were also tested in VERDI and demonstrated good timing resolution [4]. However, the strongly varying quality of sCVD diamonds precluded their large-scale implementation [4]. The anticipated TOF and energy resolutions in VERDI, 85 ps (one σ) and $\Delta E/E = 0.3\%$, respectively, are sufficient to achieve the desired mass-resolving power [5].

The main challenges to reach the targeted resolution are two defects in the measured velocity and energy. Heavy ions, such as FFs, typically give rise to a dense cloud of charges (plasma) in the PIPS detector material. This plasma momentarily perturbs the electric field across the detector, and, consequently, only charge carriers on the outer edge of the cloud will begin the migration, leaving the inner charges temporarily stationary. This deforms the signal development, leading to a time delay known as plasma delay time (PDT). Reported PDT values in the literature typically vary between 2 and 5 ns for FF [6]. If not accounted for, this effect may lead to an incorrect determination of the mass-distribution as well as an increase in systematic uncertainties [7]. A similar process, referred to as the pulse height defect (PHD) [6], causes a systematic error in the energy determination. The kinetic energy of the FFs is determined from the PIPS signal height, which is supposed to be proportional to the energy deposited by the fragment. However, non-ionising interactions and electron-ion recombination effects cause a non-linear reduction of the signal height. The impact of the PHD can cause up to a 10% reduction of the measured pulse heights. The PHD is more pronounced for heavy ions and quantified as a difference with light ions.

Earlier literature works report different PDT values and global trends, e.g. as a function of the ion energy and mass [8–12]. The reported functional dependence indicates that different detector types might exhibit unique behaviours, leading to an erroneous correction if directly applied to VERDI data. For instance, corrections based on the PDT systematics from Ref. [9] produced non-physical correlations between the average number of emitted neutrons and the total kinetic energy (TKE) obtained with VERDI [13]. The lack of experimental characterization motivated a dedicated campaign to investigate the systematic PDT and PHD behaviours in the detector species used in the VERDI setup [14].

The unambiguous determination of the PDT and the PHD behaviour relies on a well-determined prior knowledge of the impinging ion mass and energy. The LOHENGRIN fission-fragment recoil separator at the Institut Laue-Langevin (ILL), is an ideal device for such investigations. Fission fragments can be selected according to their mass-over-charge (A/Q) and energy-over-charge (E/Q) ratios with resolutions $A/\Delta A > 400$ and $E/\Delta E > 100$. The prior information on the energy and mass of the detected ions is used to calculate the true time that takes for the ions to go from the start section to the PIPS detector. The PDT and PHD information can be extracted by comparing the true time with the measured time and the true energy and measured energy respectively.

In this paper, we report a systematic measurement to characterise five PIPS detectors from VERDI. Data from wide mass and energy ranges are presented, to shed light on the functional dependency of both the PDT and the PHD effect [14]. In the following section, we describe the experimental setup as well as ion separation and selection. In section 3, a comprehensive overview of the data analysis is provided, including the digital signal processing. The findings are then discussed in section 4, highlighting the trends observed in the PDT and PHD. Moreover, a model parameterisation of the PDT is applied to describe the energy and mass dependencies. Finally, a sensitivity study was conducted to assess systematic errors.

2 Experiment

The PDT was determined by evaluating the difference between the measured time of the ion and the calculated time using the information of the ion's mass and energy provided by LOHENGRIN. Similarly, the PHD was obtained as the difference between the measured ion energy and the energy stipulated by LOHENGRIN. The fission-fragment recoil separator LOHENGRIN, is a unique instrument that can produce high fluxes of fission fragments with well-separated masses and energies. The combination of LOHENGRIN with a dedicated stop and start time section enabled the characterization of the PDT and PHD in a wide range of masses and energies.

2.1 Ion beam production and selection with LOHENGRIN

The Institut Laue-Langevin (ILL) in Grenoble, France, operates a high-flux research reactor. It provides an intense neutron flux, which amounts to 5×10^{14} n s^{-1}cm^{-2}, at the target position of LOHENGRIN [15]. A highly enriched ^{239}Pu target deposited on a thick titanium backing and covered with a 0.25 μm thin nickel foil [16] was used. Thermal neutron-induced fission fragments emitted into the direction of the spectrometer were separated according to velocity (v) and

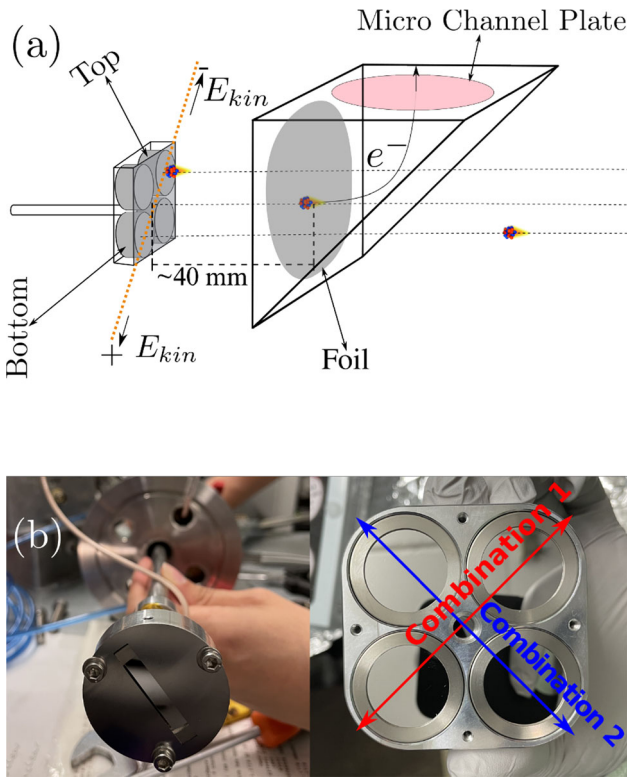

Fig. 1 Experimental setup description. **a** Schematic view of the experimental setup. A Micro Channel Plate detector (MCP) provides a start time by detecting electrons from the Al-formvar foil. The ion stop time and energy are provided by the Passivated Implanted Planar Silicon (PIPS) detectors. **b** Two different types of detector holders were used: a single holder and a clover-like holder. In the clover-like holder, the detectors were arranged in pairs (combination 1 and combination 2). All detectors used a 5 mm wide slit collimator, to filter out unwanted ion masses (not shown in the photo of the clover-configuration)

mass over charge (A/Q) ratio by the LOHENGRIN spectrometer [17].

The target used for the present experiment had been exposed to the high neutron flux already for several weeks and some of the deposited plutonium had diffused into the backing [16]. This caused additional energy loss while recoiling FFs traversing the titanium, thus effectively extending the range of accessible kinetic energies below those typical for FFs which is useful for the present purpose. The experimental campaign covered mass numbers ranging between $A = 80$ and 149 and energies between $E = 20$ and 110 MeV [16].

For integer A/Q ratios (e.g. $A/Q = 5$) more than one mass number A reaches the focal plane (e.g. $A/Q = 85/17, 90/18, 95/19$, etc.), but due to the additional selection of a fixed velocity v, ions with different masses had different kinetic energies $E = \frac{1}{2}Av^2$ and were thus identified separately by an energy-resolving detector. Hence, in the present experiment, A/Q settings were chosen to provide several masses simultaneously in the focal plane in order to measure the PDT for more mass numbers A with fewer distinct runs.

2.2 Set-up and electronics

The setup consisted of two types of detectors. The first one, a transmission detector, registered the time-of-arrival of the ions to the experimental setup. The silicon detectors acted as a stop detector for the TOF measurement. One TOF detector of the Fission Fragment Identification setup (FiFI), developed by the University of Manchester for the STEFF fission spectrometer [18], was utilized for the TOF start. The start TOF section, as shown in Fig. 1a, consisted of an emission foil, an acceleration grid, an electrostatic mirror, and an MCP detector. The foil consisted of a 25.6 nm thick aluminium coating on ~100 nm thick formvar layer. These layers were deposited on top of a 1x1 cm^2 mesh of steel wires (0.2 mm diameter). As ions traverse the foil, secondary electrons are emitted backwards and accelerated by the initial grid, positioned a few millimetres away from the foil. The electron cascade is then deflected towards the upper part of the start section by the electrostatic mirror, which was made of wires with a diameter of 20 μm. The mirror was positioned at a 45-degree angle relative to the normal plane of the foil. At the upper part of the start time section, a Hamamatsu F1942-04 MCP was mounted and operated at 2.2 kV and pressure lower than 10^{-5} Pa. The MCP had an effective diameter of 77 mm and pre-amplifies the signal internally through secondary electron multiplication.

Five Canberra time-optimised PIPS detectors of type TMPD 450 - 20NTD - 300 AM, were used in the campaign (see Table 1). The PIPS detectors had an active diameter of 23.9 mm and were operated with a nominal bias voltage of 140 V. Prior to the experiment, the impact of the bias voltage on the pulse-height spectrum was studied. The applied bias voltage was systematically varied from 130 to 149 V, without any observed effect, neither in the mean value of the measured pulse height nor the standard deviation. The PIPS detectors were mounted on a movable arm that could be manipulated externally. Two different holders were used, one hosting a single detector and another hosting four detectors in a clover configuration as shown in Fig. 1b, in which two detectors could be irradiated simultaneously. The single holder kept the PIPS detector concentrically with respect to the axis of the manipulator, which coincided with the central position of the focal plane. The position of each detector in the clover configuration was 23.5 mm off-centre with respect to the focal plane. Each detector was collimated with a 5 mm wide slit, to reduce parasitic nearby masses from entering the PIPS detector. The PIPS detectors were connected to MPR-1 Mesytec charge-sensitive pre-amplifiers, operated in a sensitivity of 200 MeV @ $\pm$ 8V, suitable for FF spectroscopy.

Table 1 List of detectors and pre-amplifiers according to their operational configuration

Detector labeling		Pre-amplifier labeling		Operation
Label	Serial nbr	Label	Serial nbr	
Top I	127699	PA II	1010125	Combination 1
Top II	127698	PA II	1010125	Combination 2
Center I	127692	PA I	0205006	–
Bottom I	127697	PA I	0205006	Combination 1
Bottom II	127694	PA I	0205006	Combination 2

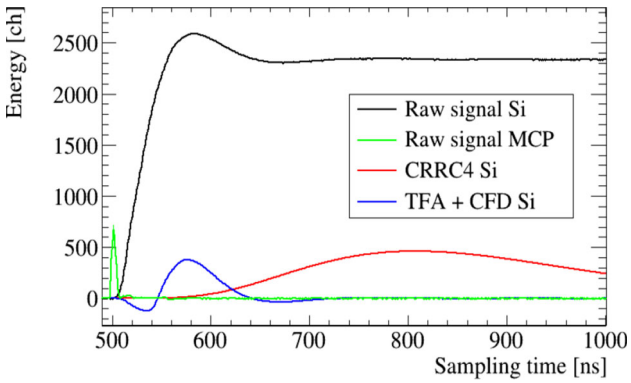

Fig. 2 Typical signals from both Micro Channel Plate (MCP) and PIPS. A CR-RC^4 digital filter was used to extract the pulse-height spectrum from the PIPS. A timing filter amplifier (TFA) was applied together with a constant fraction discrimination (CFD), in order to extract the time-pick-off from both the MCP and the PIPS detector

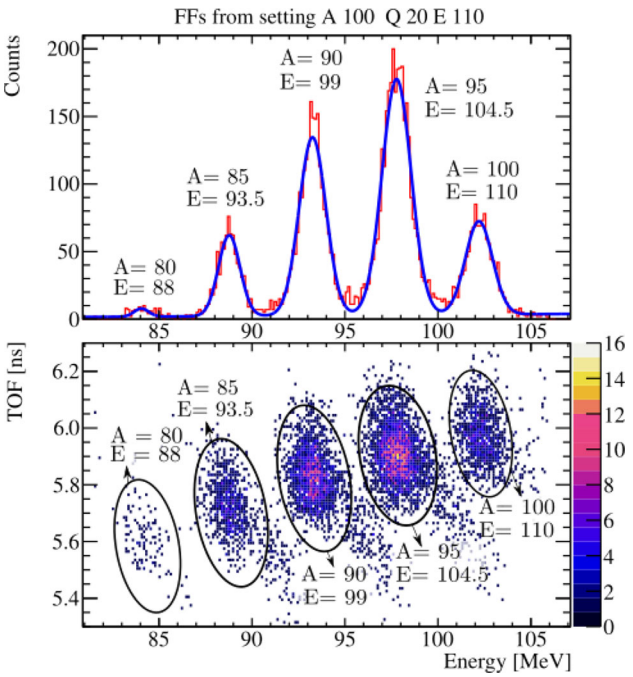

Fig. 3 Measured energy vs TOF (bottom) and projection into the energy axis (top), for the LOHENGRIN setting ($A = 100$, $Q = 20$, $E = 110$). The difference in the energy and TOF axes with the true energies and TOF for the identified FFs is due to the PHD and PDT effects. The mass is given u and the energy in MeV

The pre-amplified signals were digitised for further offline event-by-event treatment, using a SP-Devices ADQ412 waveform digitiser. The acquisition card had four channels, a sampling frequency of 1 GHz, and a 12-bit resolution. Whenever a FF triggered a signal in a PIPS channel, both the MCP and PIPS signals were recorded in a time frame of 2 μs.

3 Data analysis

The raw detector signals were treated with digital signal processing. Different digital filters were employed to optimise the time and energy resolutions. Several corrections were necessary to arrive at the true ion energy and time, e.g. energy-loss corrections, energy dispersion corrections, and spectra calibrations. In the following section, we provide a detailed description of the required analysis steps and discuss the measurement uncertainties.

3.1 Digital signal processing

Typical wave-forms from the Silicon and MCP signals are shown in Fig. 2. The MCP signal has a typical rise time of 5 ns, while the PIPS signal rise time is around 100 ns. In the first step, all traces were corrected for base-line offset and fluctuations. The ion energy was extracted from the measured pulse-height of the PIPS detectors, using a CR-RC^4 filter [19,20], with a shaping time of 600 ns. The amplitude of the resulting semi-Gaussian is proportional to the signal height.

The timing information was extracted from the PIPS and MCP detectors by applying a timing filter amplifier (TFA), followed by a Constant Fraction Discriminator (CFD). The TFA was emulated with a single digital CR-RC filter, using 10 ns both for the differentiator module (CR) and the integrator module (RC). The CFD was applied using a threshold level of 30%, and a delay of 6 ns and 30 ns for the MCP and the PIPS signals, respectively. The resulting PIPS signal is shown in blue in Fig. 2.

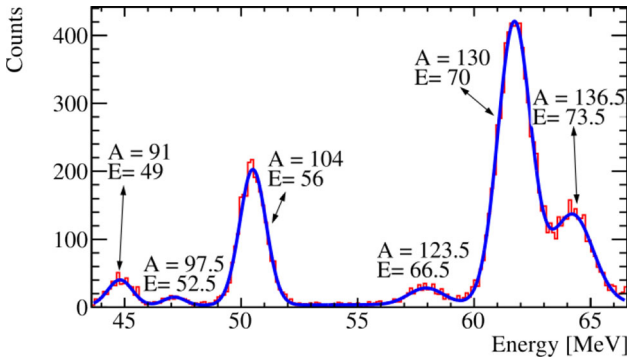

Fig. 4 Pulse-height spectrum of setting ($A = 130$, $Q = 20$, $E = 70$). The parasitic peaks identified with non-integer masses are scattered neighboring masses. The difference in the energy axis with the true energies for the identified FFs is due to the PHD effects. The mass is given u and the energy in MeV

3.2 Particle identification

Each LOHENGRIN setting allows a set of ions with common A/Q and E/Q ratios to pass through the spectrometer. A typical pulse height versus time spectrum is shown in Fig. 3, illustrating the excellent mass selection capability. The particle identification was performed by a comparison to a reference spectrum with calibrated peaks. To obtain a reference scan, the magnet setting ($A = 100$, $Q = 20$, $E = 110$) was selected, and compared to the same setting but with a modified ionic charge ($Q = 22$). Both settings contained the mass $A = 100$, at the same pulse-height channel ($E = 110$). By establishing a reference peak, the other masses could be identified by exploiting the energy-calibration and the known LOHENGRIN settings.

In the heavy mass range, some parasitic peaks with non-integer mass numbers, which theoretically should not pass the collimators, were observed in the PH spectrum. These peaks could be attributed to several phenomena, such as scattering of ions on the MCP foil, its supporting mesh, the acceleration grid, or the electrostatic mirror, all of which are located upstream of the mass-defining collimator. Scattering in these components may slightly alter the direction of ions, allowing them to bypass collimation. Additionally, significant energy losses due to the aged fissile sample could contribute to a widened beam profile, causing some ions to escape the collimation. Possible displacement or rotational misalignment of the detector collimation with respect to the beam could also play a role. For instance, one such example is observed in Fig. 4, at the setting ($A = 130$, $Q = 20$, $E = 70$), where a parasitic peak was detected despite its theoretical exclusion from the collimators. Since these non-integer peaks cannot be uniquely identified, the true ion velocity remains unknown, and they were therefore discarded in the data analysis.

3.3 Expected energy and time determination

As the ions transverse the Al-formvar foil and the dead layer of the PIPS detector, they lose some energy. In addition, four detectors were used in a clover configuration, which puts them off-centre from the central position along the beam parabola. Because of this, detected ions experience a position-dependent energy dispersion that differentiate their energies from the one provided by the LOHENGRIN E/Q ratios. As illustrated in Fig. 1a, detectors situated at the bottom position detect higher energetic ions compared with the selected E/Q ratio, whereas top detectors observe lower ion kinetic energies. The expected ion kinetic energies at the PIPS detectors were therefore determined as:

$$E = E_{\mathrm{Loh}} - E_{\mathrm{Losses}} \pm E_{\mathrm{disp}}, \tag{1}$$

where, E_{Loh} is the energy predicted by the E/Q ratio, E_{Losses} is the total ion energy loss, and E_{disp} denote the energy dispersion, which can be positive or negative depending on the position of the detectors.

The energy losses were estimated using Geant-4 (further details on the model can be found in Refs. [21–23]). Energy losses for all detected ions were simulated, in the MCP foil as well as in the PIPS dead layer. The adopted model was benchmarked with experimental stopping powers in mylar foils [24], and proved to be more accurate than the ones obtained using the SRIM package [25].

The energy dispersion implies that ions arriving 72 mm off the central position will have 1% difference in energy, compared to the E/Q value [26]. The detection set-up was positioned concentrically with the axis of the focal plane's central point (see central line Fig. 1a. In the clover configuration, the detectors centers were positioned 23.55(14) mm from the focal point. A correction for the energy dispersion was applied based on the average shift from the central position. As an example, a LOHENGRIN setting that selects ions with 100 MeV, will result in an energy dispersion of $\pm$ 0.3 MeV to either side.

The time was calculated considering non-relativistic kinematics and for a fixed distance (d), between the MCP foil and the silicon detector's surface:

$$TOF = \frac{d}{c}\sqrt{\frac{931.494 \cdot A}{2E}} = d \cdot \frac{1}{v}, \tag{2}$$

where A is the ion mass, E is the corrected ion energy in MeV and c is speed of light in m/s. The approximate value of d was around 38 mm.

3.4 Measured energy and timing resolutions

The energy resolution varied between the different detectors. The typical resolution (σ) ranges between 400 and 700 keV for the light fragments, and between 600 keV and 1 MeV for

the heavy fragments. The energy resolution (σ) of the 4.75 MeV α particles was between 17 and 25 keV, depending on the detector. The observed differences between detectors could partly be attributed to unequal noise conditions, since the electronic shielding was improved upon throughout the measurement campaign.

The combined timing resolution is measured between the MCP and the PIPS in terms of the standard deviation of the time peak (σ_t). After the digital filter optimisation, an excellent timing resolution was obtained. For the best performing detector, a time standard deviation between 60 and 80 ps was demonstrated for fission products. In comparison, the worst performing detector showed a standard deviation between 80 and 100 ps. For the α-particles, typically values were around 200 to 350 ps. VERDI will finally operate with a similar TOF setup, and is expect to reach similar resolution figures. The obtained timing resolutions for fission products set a benchmark in contemporary 2E-2v fission-fragment spectrometers and promises high-resolution mass distributions in future VERDI data.

3.5 Plasma delay time (PDT) and pulse height Defect (PHD) determination

The PDT calculations are performed by subtracting the measured TOF distribution (TOF*) from the predicted TOF:

$$PDT = (TOF^* - t_s) - TOF, \tag{3}$$

where TOF is the predicted time as calculated from Eq. 2 and t_s is a constant shift responsible for calibrating the raw digitiser time. Due to cable lengths, electronic processing and digital filtering, a constant time offset, t_s, is present in the raw TOF distribution, which is taken care of by a calibration to α particles. The time shift is found by using 4.75 MeV α particles, assuming no PDT effect for these light particles, therefore $t_s = TOF^*_\alpha - TOF_\alpha$. The resulting TOF spectrum coincides with the theoretical TOF of the 4.75 MeV α's. Following this, we shift all heavy ion TOF spectra by the same magnitude. For this purpose, a single α energy is sufficient because the digitisers ensure a sampling frequency of 1 sample/ns.

The PHD is determined in a similar fashion from the measured energies (E^*) by:

$$PHD = E - E^*, \tag{4}$$

where E is the energy postulated by LOHENGRIN, including the contributions of energy losses and dispersion. The FF energy calibration is performed relative to α's, by assuming that α-particles exhibit no PHD. Each detector measurement campaign had at least two α-particles at energies of 4.75 MeV and 12 MeV, originating from the ternary fission of ^{239}Pu and from the reaction ^{59}Ni(n, α) originated with a Ni foil covering the Pu target [17]. The measured energy of the FFs, was extracted using a linear energy calibration and a Gaussian fit of the spectrum (as in Fig. 4). The estimation of the measured energy follows the equation

$$E^* = (\alpha \cdot PH + \beta)\,. \tag{5}$$

where PH is the pulse-height (PH) channel extracted from the Gaussian fit mean value. The slope (α) and intercept (β) are obtained from the linear fit (or linear energy calibration) to the (energy, PH) coordinates extracted from α's. Each PH spectrum was fitted using the class TSpectrum of ROOT, which contains advanced spectra processing functions for one-dimensional peak search [27].

To select individual ion species we applied cuts of $\pm 2\sigma_E$, around the central value of each Gaussian peak in the pulse-height spectrum. By selecting a region of interest (ROI), the associated TOF distribution was obtained by projecting the events of the ROI onto the TOF axis.

3.6 Uncertainty estimation

We can expand Eq. (3), to expose all the sources of uncertainty for the PDT,

$$\begin{aligned} PDT &= \left(TOF^* - \left(TOF^*_\alpha - \left[d \cdot \frac{1}{v_\alpha}\right]\right)\right) - \left[d \cdot \frac{1}{v_{ion}}\right] \\ &= (TOF^* - TOF^*_\alpha) + d\left[\frac{1}{v_\alpha} - \frac{1}{v_{ion}}\right]. \end{aligned} \tag{6}$$

The flight path distance is labeled as d in Eq. (6), v_α and v_{ion} are the α's and the ions velocities respectively. The contribution or weight of each of the uncertainty components to the total PDT uncertainty was calculated by evaluating the ratio between each uncertainty component squared and the PDT variance (or PDT uncertainty squared). The flight path distance was found to be the major contributor to the total PDT uncertainty, contributing 50(20)% to the total PDT variance. The contribution of the uncertainty in the velocities due to the energy spread was negligible.

The covariance matrix of the data set was calculated using the general expression for the uncertainty propagation.

$$\boldsymbol{\Sigma}^{PDT} = \boldsymbol{J}\boldsymbol{\Sigma}^{x}\boldsymbol{J}^{T}. \tag{7}$$

Where $\boldsymbol{J}$ is the Jacobian matrix of Eq. (6)

$$\boldsymbol{J}^{x} = \begin{pmatrix} \frac{\partial PDT_1}{\partial TOF^*_1} & \cdots & \frac{\partial PDT_1}{\partial TOF^*_n} & \frac{\partial PDT_1}{\partial d} & \frac{\partial PDT_1}{\partial TOF^*_\alpha} \\ \vdots & \vdots & \vdots & \vdots & \vdots \\ \vdots & \vdots & \vdots & \vdots & \vdots \\ \frac{\partial PDT_n}{\partial TOF^*_1} & \cdots & \frac{\partial PDT_n}{\partial TOF^*_n} & \frac{\partial PDT_n}{\partial d} & \frac{\partial PDT_n}{\partial TOF^*_\alpha} \end{pmatrix},$$

and Σ^x is the variance-covariance matrix with the individual uncertainties per point in the data set,

$$\boldsymbol{\Sigma}^x = \begin{pmatrix} \sigma^2_{TOF^*_1} & 0 & \cdots & 0 & 0 \\ 0 & \sigma^2_{TOF^*_2} & \cdots & 0 & 0 \\ \vdots & \vdots & \ddots & \vdots & \vdots \\ 0 & 0 & \cdots & \sigma^2_d & 0 \\ 0 & 0 & \cdots & 0 & \sigma^2_{TOF^*_\alpha} \end{pmatrix}.$$

The diagonal elements of the PDT covariance matrix are

$$\sigma_{PDT} = \sqrt{(\sigma_{TOF^*_i})^2 + \left(\frac{1}{v_\alpha} - \frac{1}{v_{ion}}\right)^2 \sigma^2_d + (\sigma_{TOF^*_\alpha})^2}. \tag{8}$$

The PHD uncertainties, as well as each component's contribution to the total PHD variance, were calculated in an analogous way to the PDT uncertainties. Following Eq. (1), Eq. (4) and Eq. (5) the diagonal elements of the PHD covariance matrix are

$$\sigma_{PHD} = \sqrt{(\sigma_E)^2 + \underbrace{(\alpha \cdot \sigma_{PH})^2 + (\sigma_\alpha \cdot PH)^2 + (\sigma_\beta)^2}_{\sigma_{E^*}}}. \tag{9}$$

Where:

1. σ_E: Following Eq. (1), the contributors of σ_E are $\sigma_{E_{\text{disp}}}$ and $\sigma_{E_{\text{Losses}}}$. The contribution of $\sigma^2_{E_{\text{disp}}}$ to the PHD uncertainty was ruled out because its weight with respect to the PHD variance is $< 0.5\%$. On the other hand, in average, $\sigma_{E_{\text{Losses}}}$ weights 40(1)% of the PHD variance.
2. In the terms contained under σ_{E^*}, the component σ_{PH} is the uncertainty of the PH channel extracted from the Gaussian fit, its contribution to the PHD variance is $<$ 0.6%. The components σ_α and σ_β are the uncertainties of the slope and the intercept of the linear energy calibration. The contribution of the energy calibration (or $(\sigma_{E^*})^2$) to the PHD variance is 59(1)%.

4 Results and discussions

The measured PDT and PHD values relative to α particles are presented in Fig. 5a and b, as an example for one detector. We observe a strong positive correlation between the plasma delay time and the ion energy. The PDT is around 1.2 ns for the lowest energies, and reach about 3.5 ns for the highest energies studied. The increase is more than 3 ns across the energy range, and appears to start saturating around 100 MeV. This positive correlation is attributed to the creation of a larger plasma cloud at higher kinetic energies, which causes greater disruption in the detector's electric field, further delaying the motion of charge carriers. In contrast to the strong energy correlation, a weak negative mass-dependence, where heavier masses seem to exhibit smaller PDT values, is observed across the studied mass range.

In the same figure, one can study the complementary pulse-height defect trends. The PHD also exhibits a strong energy-dependency. Across the studied energy range, the PHD grows from 2 up to 8 MeV. A clear difference compared to the PDT is the mass-dependence, which seems to be pronounced in the case of PHD. For instance, ions with a fixed energy of $E = 60$ MeV, experience PHDs values ranging from 3 to 7 MeV, depending on the ion mass.

4.1 Detector intercomparison

A primary objective of this study was to determine whether the type of detectors used in VERDI exhibit consistent PDT and PHD trends. Confirming this consistency across detectors is important, as it enables a semi-global correction of the PDT for the numerous PIPS detectors used in VERDI. Five PIPS detectors were evaluated in parallel to identify any systematic discrepancies among them. Representative results for masses $A = 85$, 95, 130 and 143 are shown in Fig. 6.

In general, all studied detectors exhibited similar PDT and PHD trends. In terms of energy and mass dependence, we observed the same behavior from all of them. In Fig. 6, three detectors (Central I, Bottom I, Bottom II), exhibited overlapping PDT trends within uncertainty limits. Detector Top I, deviated from the rest for ions in the low mass region for energies higher than 70 MeV, but presented overlapping values for higher masses, even for energies higher than 70 MeV. Detector Top II, experienced a constant shift toward lower PDT values. In spite of this, detector Top II preserved the functional dependency exhibited by detectors Central I, Bottom I and Bottom II. Thus, one could correct for these types of discrepancies on average. In the correction procedures of future VERDI data, every detector has to be calibrated and benchmarked to known velocity data, by-fine-tuning the PDT correction while preserving the general trends of the PDT behavior as a function of mass and energy.

The following section presents sensitivity analysis results, demonstrating that the observed discrepancies between detectors do not suggest any unresolved systematic effects that could compromise the validity of these findings.

4.2 Sensitivity analysis

A sensitivity analysis was conducted to assess the direct impact of primary uncertainty sources on the calculated PDT and PHD values, focusing on factors identified as major contributors in the uncertainty analysis (Sect. 3.6), including energy-loss calculations, flight-path distance measurement

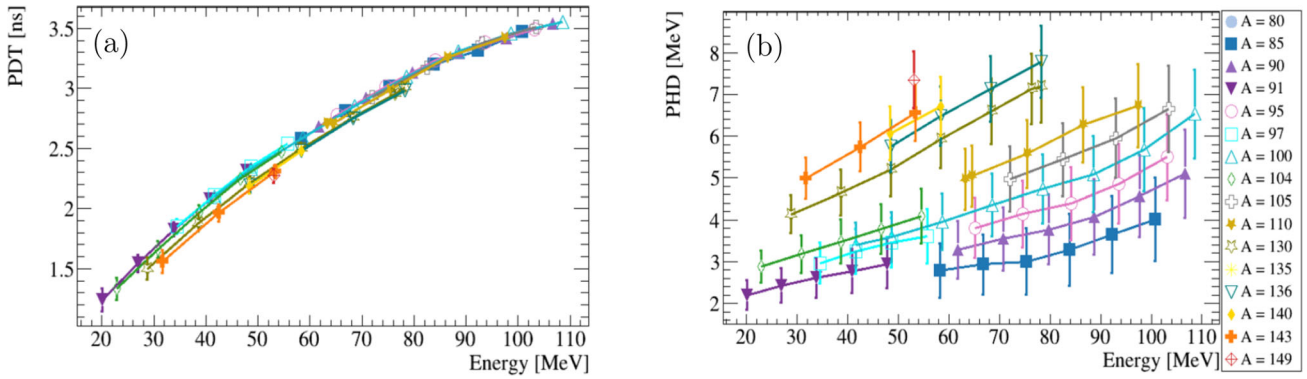

Fig. 5 PDT and PHD measured with detector Bottom I. The PDT has been calculated relative to α's of 4.75 MeV and the PHD has been calculated relative to αs of 4.75 MeV and 12 MeV. **a** Plasma delay time (PDT) as a function of the energy for different masses. **b** Pulse height defect (PHD) as a function of the energy for different masses

errors, and calibration accuracy. While these factors contribute significantly to the total uncertainty, when compared to other sources of uncertainty, varying them within their estimated ranges introduces only minor shifts in PDT and PHD values. These shifts remain within overall uncertainty limits. Additional sensitivity studies were performed by varying the high-voltage, and the parameters of the digital signal filtering for the time pick-off determination.

4.2.1 Influence of energy losses

The thickness of the formvar layer of the MCP foil was estimated with an uncertainty of 50% [28]. We assessed the impact of this uncertainty on energy-loss calculations using Geant4 simulations. The PDT and PHD values were recalculated assuming $\pm 50\%$ variation in the formvar layer thickness.

As shown in Fig. 7a, the effect on PHD values for $A = 85$ was found to range from 0.5 to 1 MeV, depending on the energy. Despite this variation, the resulting PHD values remained within acceptable uncertainty limits. Similarly, the PDT values showed a minor shift of approximately 50 ps, well within the uncertainties.

Although target inhomogeneities could potentially contribute to inter-detector discrepancies in PHD-assuming that detectors at the bottom face a region with 50% thicker foil and those at the top face a thinner region-the observed effect on PDT is too small to explain the differences seen in Fig. 6. This suggests that inhomogeneities in the formvar layer are not the primary cause of the inter-detector discrepancies in PDT.

4.2.2 Effects due to calibration issues

Each detector has a unique energy calibration, which could theoretically contribute to inter-detector discrepancies. However, the observed differences in PHD and PDT between detectors are consistent with expected uncertainty levels, suggesting that calibration-related uncertainties do not significantly contribute to the discrepancies seen in Fig. 6.

As mentioned in Sect. 3.5, the energy calibration was performed assuming negligible PHD for α-particles. Although α-particles exhibit a small PHD, it is much smaller than for FFs, and this analysis focuses on relative differences. During the linear energy calibration, an extrapolation from the low-energy regime of α-particles to the high-energy regime of FFs was performed. Sensitivity analysis showed that small uncertainties in the calibration slope α in Eq. (5), could lead to an offset of up to 1 MeV in the PHD values, as illustrated in Fig. 7.(b). However, this offset remains within the overall uncertainty range of our measurements.

4.2.3 Effects due to flight path distance uncertainty

Sensitivity analysis with deviations of 1 mm and 3 mm in the flight path distance (see Fig. 7c) showed that the effect on PDT values was minor, with changes remaining within the overall uncertainty limits. Although the flight path distance was identified in Sect. 3.6 as a major contributor to PDT uncertainty compared to other sources, its practical impact on PDT values was insufficient to explain the observed inter-detector discrepancies. The flight path distance was determined by measuring various setup components, with uncertainties arising from systematic sources (instrument resolution) and statistical sources (repeated measurements), resulting in an average uncertainty of 1.1 mm. Additionally, ion scattering after passing through the MCP foil introduced an estimated deviation of 2.8 mm, based on the maximum scattering angle that still allows the ion to be detected given the detector and collimation dimensions.

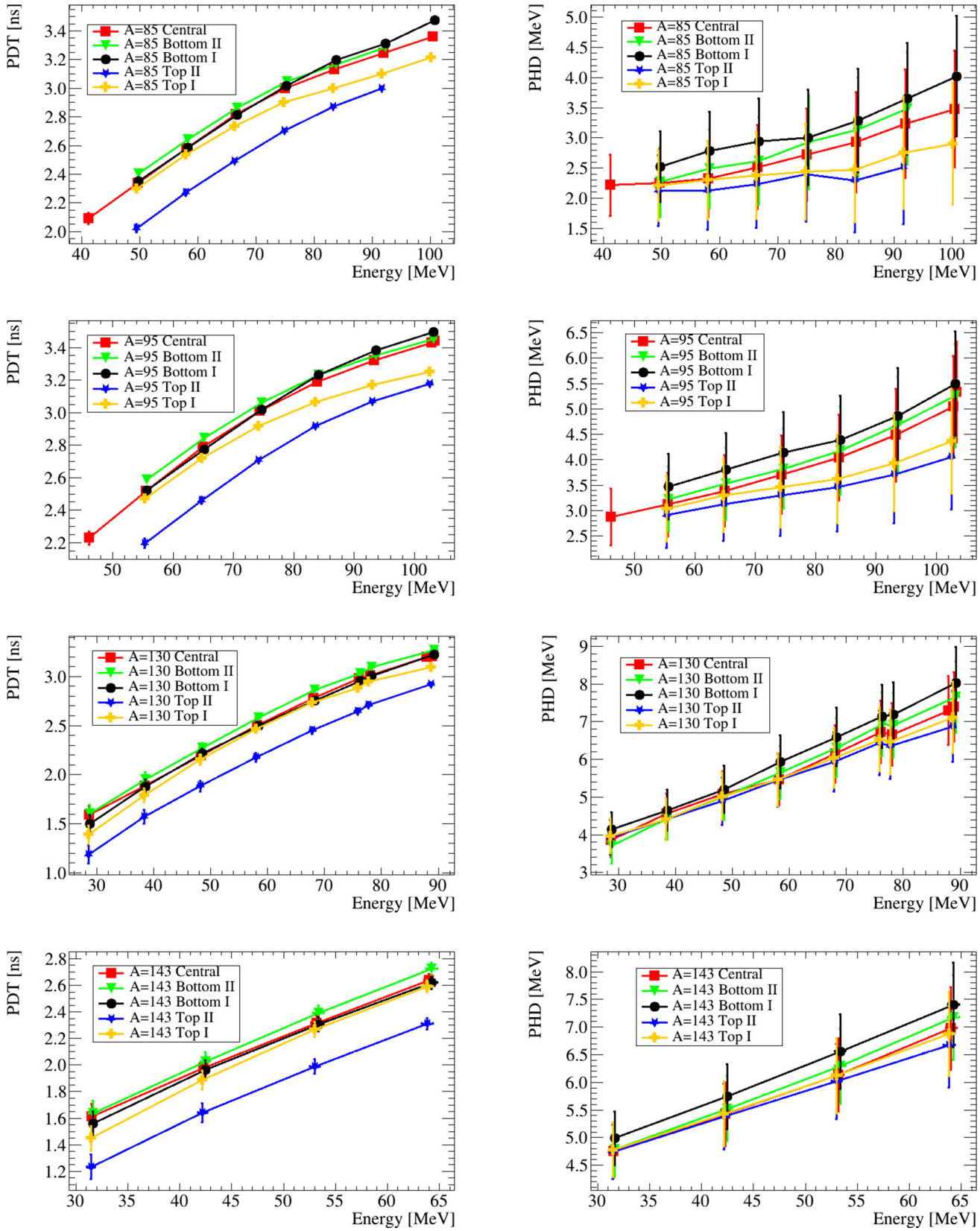

Fig. 6 Inter-detector comparison of plasma delay time (left) and pulse height defect (right) for the masses $A = 85$, 95, 130, and 143. The eye-guiding lines indicate a linear interpolation between the measurements. The PDT has been calculated relative to αs of 4.75 MeV and the PHD has been calculated relative to αs of 4.75 MeV and 12 MeV

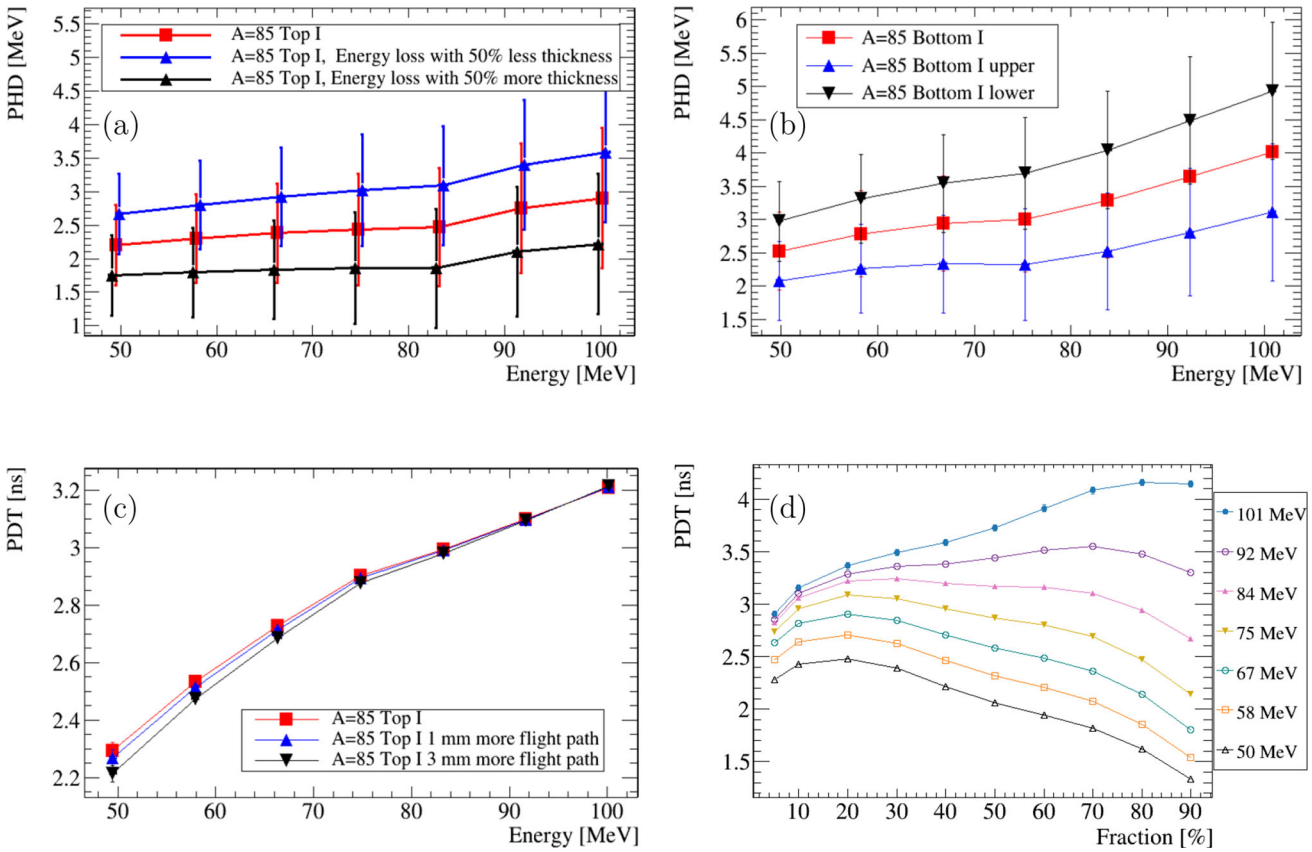

Fig. 7 Sensitivity analysis performed on a selected ion ($A = 85$) to study systematic uncertainties. **a** PDT values calculated for energy losses calculated at different foil thicknesses to study the impact of target inhomogeneities. Even for a maximum variation in the foil thickness, the PHD values still overlap within uncertainty limits. **b** PHD values incorporating errors in the linear energy calibration factors labeled as σ_a in Section 3.6. The label upper means the PHD value calculated with $a + \sigma_a$ and lower means $a - \sigma_a$, **c** PDT trends calculated with different TOF distances to study the impact. Even for a variation of 3 mm in the flight path, the resulting PDT values still overlap within uncertainty limits with the other trends, ruling out possible impacts due to ion scattering. **d** The PDT at different settings for the Constant Fraction Discriminator of ion (A = 85) in all available energies (see legend on the right) for detector Bottom I.

4.2.4 The role of digital filters

The implemented digital filters turned out to play a rather important role for the deduced PDT values. Depending on the chosen settings, one could affect the PDT by a large amount. Figure 7d shows a systematic variation of the CFD trigger level fraction, as an example for A=85. The variation in PDT values grow as a function of the chosen CFD fraction. Thus it is necessary to use a common, and rather low, CFD trigger level. A fraction level of 30% was selected to optimize the TOF resolutions, and will be used in future works on VERDI.

5 Model parameterisation

While we present an extensive data-set, for a wide range of ions and energies, it is important to generalise our findings by comparing our functional dependencies with earlier literature studies. In order to do so, we performed a two-dimensional fit of our experimental data.

5.1 Previous studies

Several semi-empirical parameterisations have been proposed to describe the PDT. Here we discuss a limited number of models, which have been mentioned in earlier works.

Bohne et al. [8] propose a model with two distinct operational regions based on the effective field strength (F_{eff}) of the detector: region I, where F_{eff} exceeds a critical value F_{min}, and region II where $F_{eff} < F_{min}$. In Region I, the PDT is suggested to decrease with the energy and mass of the ion, following the proportional relation $PDT \propto e^{-E/A}/(2A)$. For region II, they propose a non-linear relationship where the PDT increases according to $PDT \propto (A^2) \ln(2E) e^{-E/A}$. Bohne et al. [8] parametrisation was developed to characterize the PDT in experimental data of ions ranging from ^{12}C

Table 2 Compared PDT models

Model name	Equation
Proposed model	$PDT(A,E) = p_0E + p_1E^2 + p_2\frac{A^2}{E} + p_3E^{\frac{1}{2}}A^{-\frac{1}{6}} + p_4$
Neidel	$PDT(A,E) = E^{b_0}A^{b_1}b_2$

to ^{129}Xe, with energies between 55 MeV and 480 MeV, relative to α's of 8.78 MeV. Their measurements were performed using surface barrier detectors manufactured by ORTEC with operation voltage biases between 100 V to 275 V.

Neidel et al. [11] propose a parametrisation where the PDT increases with the square root of the detected ion's energy and the sixth root of its mass, expressed as $PDT \sim \sqrt{E}A^{1/6}$. This model was formulated based on experimental measurements involving fission fragments and alpha particles from ^{252}Cf, and it compared the PDT in self-fabricated and ORTEC surface barrier silicon detectors operated at a bias voltage of 70 V.

A third model proposed by Seibt et al. [10], uses a weaker energy dependency of the PDT, amounting to the power of 1/3, and no dependence on the ion's mass. This model was developed for light ions from ^{252}Cf (A = 4, A = 16) in energies between 5.3 MeV and 42 MeV and FFs with an average energy of 90 MeV using silicon surface barrier detectors operated with voltage biases between 4 V and 300 V.

These models were evaluated by performing fits to our experimental data. The parameterizations proposed by Bohne et al. [8] and Seibt et al. [10] did not accurately describe the trends observed in our data. In contrast, the parameterization by Neidel et al. [11] provided a more accurate description of the PDT in our detectors and it was further analyzed.

5.2 PDT parameterisation

A complete theoretical modeling of the plasma delay time is beyond the scope of this work. In order to properly describe this phenomenon, one needs to consider many factors. For instance the stopping power of all possible fission fragments, the time-dependent effective charge distribution of the ions, the detector material properties (resistivity, capacitance, field strength, etc). Instead, we resort to an empirical parameterisation of the experimental data, to reveal mass- and energy dependence. All fit parameters were optimised by performing a global fit on all data from the five detectors. The results for each model were tested by calculating the residual of each PDT measurement point to the result of its model prediction $PDT(A,E)$.

First we attempted to apply earlier literature models to describe our data. One such attempt was based on the Neidel model as shown in Table 2. This function is an inspired parametrical representation of the PDT function proposed by Neidel et al. [11], based only on three parameters, which in our case were free fit parameters, whose global fit values were $b_0 = 0.60(9)$, $b_1 = -0.059(18)$, $b_2 = 0.28(3)$. For this model, a systematic deviation with respect to energy and mass was found (see the left side of Fig. 8). The residuals increase proportionally with the ion energy, positively for $E < 60$ MeV and negatively for $E > 60$ MeV. Moreover, the residuals for higher masses are systematically shifted towards lower values. The mean values of all the residuals across all detectors range from −242 ps to 124 ps, with the maximum deviation from the experimental data reaching 500 ps, significantly outside the TOF resolution limits between 60 ps and 100 ps. The standard deviation across detectors was between 63 ps and 104 ps.

We sought a new empirical parameterisation, with more parameters to better describe the experimental data. This newly developed function, which is valid in the energy and mass regime of FFs, is outlined in Table 2. By performing a global fit to the data, we obtained coefficients specified in Eq. (10). A 3D view of the proposed model is shown in the bottom plot of Fig. 9. The residual distributions for this model are shown on the right side of Fig. 8. For detector Central I (top right corner in Fig. 8), the residuals for higher masses (yellowish points) are not consistently shifted towards lower values. Additionally, the majority of the residual points for detector Central I, are constrained to a range of 100 ps, in contrast, the residuals for Neidel's model, are contained in a range of 250 ps. For detector Top II (bottom right corner in Fig. 8), the proposed model significantly reduces the residuals, constraining them within a range no larger than 140 ps, compared to the Neidel model, where the residuals expand to a range of nearly 400 ps. For all detectors, the residual distributions presented an improvement in the standard deviations, resulting in a reduction of around 50%. The mean residual value across all detectors ranged between −8 ps and 68 ps, with a maximum standard deviation of 48 ps and a minimum of 29 ps. The most prominent outliers were observed at low masses, where fewer events were detected. Overall, the majority of residual points across detectors remain within the TOF resolution.

$$PDT(A,E) = 0.05(5)E - [(1.62(15)) \times 10^{-4}]E^2 - [(5.8(12)) \times 10^{-4}]\frac{A^2}{E} - 0.02(3)\frac{\sqrt{E}}{A^{1/6}} + 0.62(9) \quad (10)$$

Figure 10 shows the individual fits applied to each detector using the proposed model in Table 2, as well as the param-

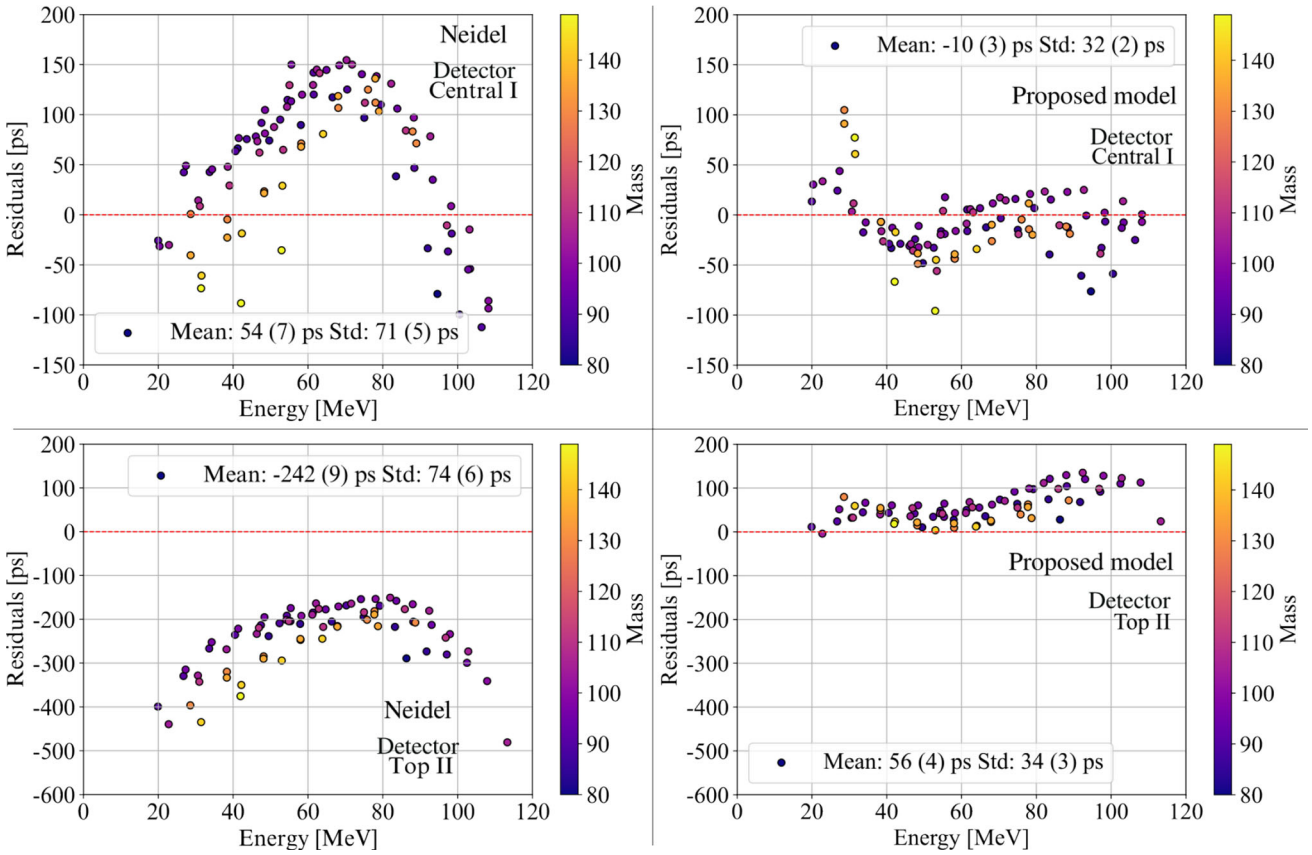

Fig. 8 Residual distributions as a function of the energy of the incident ion for all detected masses. The residuals are the difference between the PDT model prediction and the experimental points for two selected cases. The residuals shown on the left side are those of the Neidel-inspired model, while on the right side are the residuals from the evaluation of our proposed model

eters from the global fit resulting in Eq. (10) (dashed lines). Calculating the residuals from each individual fit gave a standard deviation between 20 ps and 30 ps, which in all cases is within the timing resolution limits.

A comparison of the fits using the two models under study is shown in the upper plot of Fig. 9. The dashed lines represent the Neidel-inspired model, and the solid lines denote our proposed parameterisation. In the lower and high mass ranges, the residuals for the Neidel model have clear deviations exceeding the uncertainty bars present at higher masses, notably at $A = 130$. For this mass, significant deviations are evident for the Neidel model at energies above 80 MeV, unlike the smaller deviations seen at $A = 85$ within the same energy range, indicating an underestimation of the mass dependence. The Neidel model also shows slightly higher deviations from the experimental data at $A = 143$ compared to $A = 130$ at energies below 60 MeV. On the other hand, the present model consistently provides more accurate predictions of the experimental data across all scenarios.

6 Conclusions

We have reported on an extensive investigation of the plasma delay time and pulse height defect in PIPS detectors. The LOHENGRIN fission-fragment recoil separator provided mass- and energy-selected fission fragments for the characterisation of five PIPS detectors.

The PDT was found to have a strong positive correlation with the ion energy and a weaker and negative correlation with the mass. The experimental PDT values determined from five detectors confirm a systematic behavior with respect to mass and energy, although one detector showed a systematic shift towards lower PDT values. Such inter-detector discrepancies can be accounted for by allowing the proposed new PDT parametrization to have more flexibility in the iterative calibration procedures to correct the PDT on the VERDI 64 PIPS detectors.

A sensitivity analysis was performed to assess the systematic uncertainties of the measured data. This includes e.g. the uncertainties in foil thickness, faulty calibrations, errors in the measured flight-path distance, digital filter implica-

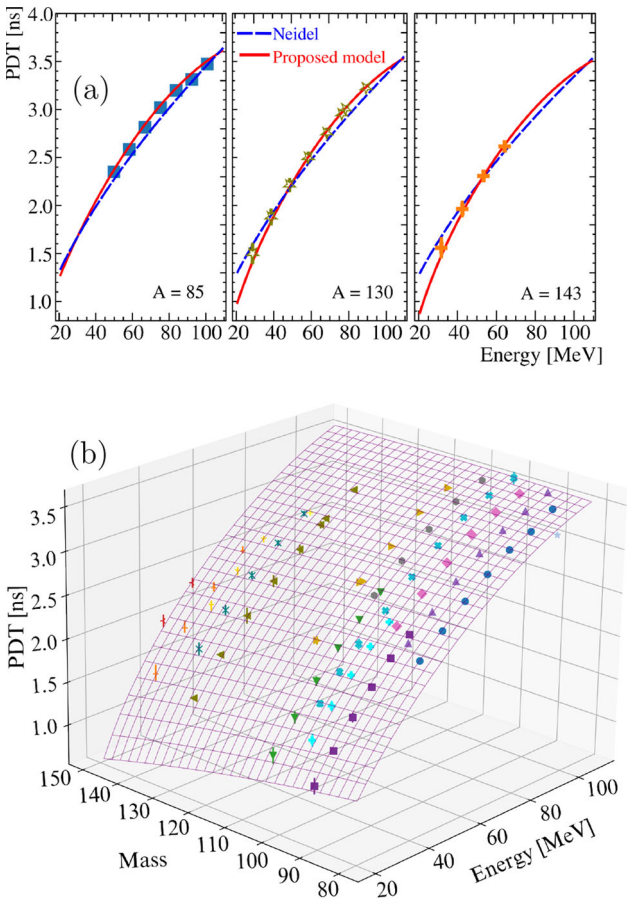

Fig. 9 Three dimensional view of the PDT fit plane and some projections. **a** PDT vs Energy for detector Bottom I and fit to three representative masses. The solid lines represent the fit using our proposed model in Table 2 the dashed line corresponds to the Neidel model prediction of Table 2. **b** PDT data as a function of mass and energy and fit plane following our parameterised model (see Eq. (10))

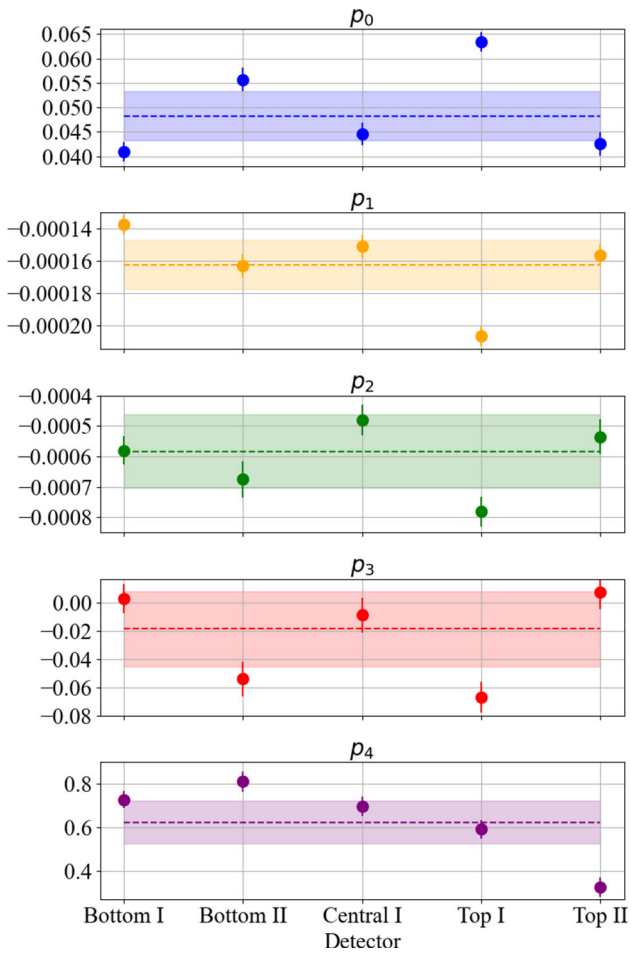

Fig. 10 Fit parameters results from the two-dimensional regression using our proposed model (see Table 2) to the PDT data of each detector (dots) and results from global fit using all detectors (dashed lines for values and shadow areas for uncertainties)

tions as well as variations in the bias voltage. After varying these factors within their estimated ranges the resulting PDT measurement presented only a minor shift within uncertainty limits.

We have attempted to identify a suitable parameterization for describing our PDT data, as previous literature functional dependencies proved insufficient for our needs. We propose a new PDT parametrization as outlined in Eq. 10, albeit a bit more complicated than previous literature models. The model, which is valid in the FF energy and mass regime, infers generally that the PDT increases with energy and decreases with mass. While a simpler and more accurate function may be discovered in the future, potentially more founded in physical considerations, we are satisfied with the current model to correct VERDI velocities. The model achieves a better precision than the experimental resolution of our velocity data, making it a good compromise. Note that the final VERDI data will require fine-tuning of the PDT parameters for each detector to accurately reproduce known standard calibration fission data. While the current model parameters provide a global ansatz that effectively describes the bulk of the data, we intend to allow the model some flexibility to account for individual detector characteristics.

In the near future, we plan to verify the newly developed PDT parameterisation by applying it to fission-fragment data previously taken with the VERDI spectrometer. By providing a consistent PDT correction to the TOF data, we may expect a significant improvement of VERDI's mass resolution.

Acknowledgements This work was supported by the Swedish Research Council (VR ref. no. 2019-05385) and by the Swedish Centre for Nuclear Technology (SKC). This project has received funding from the Euratom research and training programme 2014–2018 under grant agreement No 847594 (ARIEL). This work is part of the MÅSTE project (P202301281), supported by the Swedish Energy Agency. A.A. would like to acknowledge Ingegerd Berghs stiftelse and Carl Tryggers stiftelse for the research grants. Special thanks go to S.J. Holm for his technical support. The co-authors from the University of Manchester and the University of Edinburgh would like to thank Andrew Mcfarlane.

This work includes data obtained at the ILL under DOI 10.5291/ILL-DATA.3-01-694.

Author contributions Ana M. Gómez L.: Experimental preparations and execution, software development, data analysis, writing-original draft. Ali Al-Adili: Experimental proposal, funding acquisition, experimental preparations and execution, supervision, data analysis, writing-review and editing. Diego Tarrío: Supervision, data analysis, writing-review and editing. Andreas Solders: Supervision, data analysis, software development, cross-checking results, writing-review and editing. Zhihao Gao: Experimental participation, software development. Alf Göök: Experimental participation, data validation, writing-review and editing. Stephan Pomp: Project supervision, writing-review and editing. André Poussette: Data analysis. Samuel Bennet: Experimental participation, writing-review and editing. Yung Hee Kim: Data analysis expertise, consultation. Ulli Köster: Experimental preparations and execution, data analysis support, writing-review and editing. Andreas Oberstedt: Writing-review and editing. Gavin Smith: Development of TOF section. Nikolay V. Sosnin: Development of TOF section, data analysis support, writing-review and editing. Stephan Oberstedt: Supervision, data analysis, writing-review and editing.

Funding Open access funding provided by Uppsala University.

Data Availability Statement This manuscript has no associated data . [Author's comment: There are data sets generated and analyzed at this article. Part of the generated data is presented in the plots. Further data can be shared at reasonable request.]

Code Availability Statement This manuscript has no associated code/software. [Author's comment: There is code/Software generated for this article and can be shared at a reasonable request.]

References

1. M.O. Frégeau et al., First results from the new double velocity-double energy spectrometer verdi. Nucl. Instrum. Methods Phys. Res. Sect. A 817:35 (2016)
2. K. Jansson et al., The new double energy-velocity spectrometer verdi. EPJ Web Conf. **146**, 04016 (2017)
3. A. Al-Adili et al., Prompt fission neutron yields in thermal fission of ^{235}U and spontaneous fission of ^{252}Cf. Phys. Rev. C **102**, 064610 (2020)
4. M.O. Frégeau et al., First use of single-crystal diamonds as fission-fragment detector. Nucl. Instrum. Methods Phys. Res. Sect. A **791**, 58–64 (2015)
5. M.O. Frégeau et al., The fission-fragment spectrometer verdi. Phys. Procedia **64**, 197–203 (2015). Scientific Workshop on Nuclear Fission Dynamics and the Emission of Prompt Neutrons and Gamma Rays, THEORY-3
6. G.F. Knoll, Radiation Detection and Measurement. Wiley, New York, pp. 385, 389, 393 (2000)
7. A. Al-Adili et al., Studying fission neutrons with 2e–2v and 2e. EPJ Web Conf. **169**, 00002 (2018)
8. W. Bohne et al., The influence of plasma effects on the timing properties of surface-barrier detectors for heavy ions. Nucl. Instrum. Methods Phys. Res. Sect. A **240**, 145 (1985)
9. J. Velkovska et al., Fission fragment mass reconstruction from si surface barrier detector measurement. Nucl. Instrum. Methods Phys. Res. Sect. A **430**, 507 (1999)
10. W. Seibt et al., Charge collection in silicon detectors for strongly ionizing particles. Nucl. Inst. Methods **113**, 317 (1973)
11. H.-O. Neidel et al., Plasma delay of ^{238}U ions in surface barrier detectors. Nucl. Instrum. Methods Phys. Res. **212**, 299 (1983)
12. S. Aiello et al. Plasma effects for heavy ions in implanted silicon detectors. *Nucl. Instrum. Methods Phys. Res., Sect. A*, 427:510, (1999)
13. K. Jansson, *Measurements of Neutron-induced Nuclear Reactions for More Precise Standard Cross Sections and Correlated Fission Properties*. Phd thesis, Uppsala University, (2017)
14. A.M. Gómez-L et al., Determination of the plasma delay time in pips detectors for fission fragments at the lohengrin spectrometer. EPJ Web of Conf. **284**, 04012 (2023)
15. S. Oberstedt et al., Light charged particle emission in the reaction ^{251}Cf(n_{th}, f). Nucl. Phys. A **761**, 173 (2005)
16. U. Köster, et al. Experience with in-pile fission targets at lohengrin. *Nucl. Instrum. Methods Phys. Res., Sect. A*, 613:363, (2010)
17. U. Köster et al., Ternary fission yields of ^{241}Pu(n_{th}, f). Nucl. Phys. A **652**, 371 (1999)
18. A.J. Pollitt et al., Measurements of energy and multiplicity from 235u(nthermal) using steff. EPJ Web Conf. **93**, 02018 (2015)
19. A. Al-Adili, Measurements of the ^{234}U (n,f) Reaction with a Frisch-Grid Ionization Chamber up to E_n =5 MeV. Phd thesis, Uppsala University, (2013)
20. Al-Adili A., et al. Comparison of digital and analogue data acquisition systems for nuclear spectroscopy. *Nucl. Instrum. Methods Phys. Res., Sect. A*, 624:684, (2010)
21. A. Al-Adili et al., Simulations of the fission-product stopping efficiency in igisol. Eur. Phys. J. A **51**, 59 (2015)
22. K. Jansson et al., Simulated production rates of exotic nuclei from the ion guide for neutron-induced fission at igisol. Eur. Phys. J. A **53**, 243 (2017)
23. Z. Gao et al., Benchmark of a multi-physics monte carlo simulation of an ion guide for neutron-induced fission products. Eur. Phys. J. A **58**, 27 (2022)
24. T. Materna et al., Stopping power of fission fragments in thin mylar and nickel foils. Nucl. Instrum. Methods Phys. Res., Sect. B **505**, 1 (2021)
25. A. Pousette , Simulations of energy losses of fission fragments in mylar foils at lohengrin, (2023)
26. P. Armbruster et al., The recoil separator lohengrin: Performance and special features for experiments. Nucl. Inst. Methods **139**, 213 (1976)
27. M. Morháč, et al. Background elimination methods for multidimensional coincidence γ-ray spectra. *Nucl. Instrum. Methods Phys. Res., Sect. A*, 401:113, (1997)
28. N.V. Sosnin, *Atomic Number and Gamma-ray Measurements from Neutron-induced Fission at the ILL and* n_{ToF}. Phd thesis, Manchester University (2020)